Hindawi Publishing Corporation
International Journal of Photoenergy
Volume 2012, Article ID 151452, 11 pages
doi:10.1155/2012/151452

Research Article

Optimal *I-V* Curve Scan Time of Solar Cells and Modules in Light of Irradiance Level

Matic Herman, Marko Jankovec, and Marko Topič

Laboratory of Photovoltaics and Optoelectronics, Faculty of Electrical Engineering, University of Ljubljana, Tržaška Cesta 25, 1000 Ljubljana, Slovenia

Correspondence should be addressed to Matic Herman, matic.herman@fe.uni-lj.si

Received 3 June 2012; Revised 7 October 2012; Accepted 25 October 2012

Academic Editor: Wayne A. Anderson

High-efficiency solar cells and modules exhibit strong capacitive character resulting in limited speed of transient responses. A too fast *I-V* curve measurement can thus introduce a significant error due to its internal capacitances. This paper analyses the *I-V* curve error of a measured solar cell or module in light of scan time and irradiance level. It rests on a two-diode solar cell model extended by two bias-dependent capacitances, modelling the junction, and the diffusion capacitance. A method for determination of all extended model parameters from a quasistatic *I-V* curve and open-circuit voltage decay measurement is presented and validated. Applicability of the extended model and the developed parameter extraction method to PV modules is demonstrated and confirmed. SPICE simulations of the extended model are used to obtain the *I-V* curve error versus scan time dependence and the *I-V* curve hysteresis. Determination of the optimal scan time is addressed, and finally the influence of the irradiance level on the *I-V* curve scan time and error is revealed. The method is applied but is not limited to three different wafer-based silicon solar cell types.

1. Introduction

The *I-V* curve measurement is an essential performance characterization technique for solar cells and modules as two-terminal DC generators. Either in dark or under illumination, the measurement concept is simple: during the sweep of the terminals of the device under test (DUT) from open circuit to short circuit or vice versa, voltage and current should be measured in quasi static conditions. It can be mistakenly assumed that PV generators exhibit negligible internal capacitance. In particular, the last generation thin film solar cells (SCs) and high-efficiency crystalline silicon SCs exhibit extremely high internal capacitances [1]. The internal capacitance together with the series, parallel, and diode differential resistance form an RC circuit that introduces a transient time constant into the measurement process. The time constant determines the quasi static condition. Its magnitude depends on various parameters such as the operating point (voltage and current), temperature, irradiance level, minority carrier lifetime, and other semiconductor parameters only to mention the most important ones.

While sweeping the *I-V* curve from point to point, the transient behaviour needs to fade out prior to the measurement being error-free. The charge of the capacitor in the DUT needs to equalize at every point of the measurement. An inappropriate *I-V* scan time can introduce a significant error into the *I-V* measurement. When the targeted error is to be kept below a predefined threshold, the *I-V* curve scan time is downward limited and determined by the SC's dynamic properties. On the other hand, there are several factors determining the scan time upper limit. Foremost, the scan time is dictated by the *I-V* curve measurement device. For resistive/semiconductor-based curve tracers, the upper limit is defined by the safe operating area (SOA) of the load (usually an MOSFET). For capacitive curve tracers, the capacitor charging time is a fixed quotient of the measurement load capacitance and the current capabilities of the DUT. At indoor measurements, the *I-V* curve scan

time is upward limited by the duration of homogenous light pulse guaranteed by a flash solar simulator. Measurements under a continuous solar simulator or under the sun can further suffer from errors induced by radiation heating of the specimen [2]; thus, the scan time should not be too long.

To sum up, the optimal scan time should be as short as possible but long enough for the dynamic error to be kept below the predefined error threshold. A too short scan time can be easily detected by scanning the curve in both directions [3]: forward—a scan from short circuit current I_{SC} to open circuit voltage V_{OC}; reverse—from V_{OC} to I_{SC}. A hysteresis can be observed demonstrating underestimation of the real I-V curve in the forward direction and overestimation in the reverse direction (Figure 1(a)).

The resulting error cannot be eliminated neither by averaging both I-V curves by voltage nor summing the errors (determined by the error function given in Section 2) of both scan directions (Figure 1(b)). In particular, at too short scan times, the mismatch is high due to $R_s dI/dt$ term, where R_s is the series resistance of the DUT. The term that determines the error at a fixed time constant value varies at different sweep directions [3]. Furthermore, in several cases (capacitive or inductive load), the detection of the error by sweeping in both directions is not applicable; thus, the determination of required scan time or characterization of dynamic error is even more important.

Measurements under solar simulators are based on a calibrated light source that emits as close as possible to 1000 W/m^2 as specified in the standard test conditions (STCs) [4]. However, in measurements under the sun, the irradiance levels can vary over a broad range. The IEC 60409-10 standard defines the procedures for scaling the I-V curves to STC [5], but does the irradiance level impact the I-V measurement error or is there a need for a different scan time? We will address these aspects in our quest for the optimal scan time.

The hysteresis and the effect of the capacitive character of solar cells are well known and reported [3, 6]. Several variations of the dynamic model exist, where most authors use a one-diode model including one or two capacitances [1, 6, 7], while one author uses a two-diode model and two capacitances [8]. None of the presented models were applied and verified on different solar cell technologies. Our previous research has shown that a two-diode model should be used for the optimal extraction of the junction capacitance [9]. The aim of this paper is to analyse the I-V curve error of a solar cell or module under test in light of scan time and irradiance level. The analysis is accomplished through SPICE simulation utilizing a two-diode model extended by two nonlinearly bias-dependent capacitors modelling the dynamic character of PV generators. A method for parameter extraction of the presented extended model is developed and evaluated. Whether the model suitably characterizes not only solar cells but also PV modules is discussed in theory and practice. An algorithm for scan time determination is developed, and finally the influence of the irradiance level on the I-V curve scan time and error is revealed. Results are demonstrated on three different solar cells of three different technologies: polycrystalline silicon (pc-Si), monocrystalline silicon (mc-Si) and back-contacted monocrystalline silicon (BC mc-Si).

2. Measurement and Modelling Methodology

2.1. Error Determination. The optimal scan time is the minimal time at which the error between a reference curve measured in true quasi static conditions and a curve under the influence of a transient error does not exceed a predefined error threshold. Determination of the error between the reference and the compared I-V curve is an essential yet delicate procedure that needs to be established for further analysis. The comparison of I-V curves is difficult due to the wide curve slope span (dI/dV) from I_{SC} to V_{OC}. Neither the current difference at equidistant voltage intervals nor the voltage difference at equidistant current intervals is appropriate. A possible comparison quantity is the maximum peak power P_{MPP}, although it only relates to single points on both curves and does not provide alignment information of the entire I-V curve. We suggest a method that delivers overall I-V curve comparison, with the error equally weighted throughout the curve form I_{SC} to V_{OC}.

Let the reference curve be stored in the $\mathbf{M}_{IV}$ matrix, and let the compared curve be stored in the $\mathbf{N}_{IV}$ matrix, where I denotes the current, and V denotes the voltage column of the two-column matrices. The error is derived from a perspective of the available power of the PV generator at a specified load. The points for error calculation are selected as two intersections of a variable linear resistive load characteristics and both curves being compared (ith point $\mathbf{O}_{IV}(i)$ on the reference and ith point $\mathbf{N}_{IV}(i)$ on the compared curve, Figure 2).

The characteristics of the variable resistive load is defined as $I = \mathbf{g}(i) \cdot V$. Foremost, the vector $\mathbf{g}$ is calculated as $\mathbf{g}(i) = \mathbf{N}_I(i)/\mathbf{N}_V(i)$ for each of N points of the compared curve. The reference curve is defined discretely; thus, interpolation is required. For every line $I = \mathbf{g}(i) \cdot V$ going through the $\mathbf{N}_{IV}(i)$, the intersection point on the reference curve is interpolated (1st order) from the nearest points ($\mathbf{M}_{IV}(j)$ and $\mathbf{M}_{IV}(j+1)$) and stored into the $\mathbf{O}_{IV}(i)$ matrix. Finally, the components of the error vector can be calculated from $\mathbf{N}_{IV}(i)$ and $\mathbf{O}_{IV}(i)$ point pairs:

$$\mathbf{E}(i) = \sqrt{\left(\frac{\mathbf{N}_V(i) - \mathbf{O}_V(i)}{V_{\mathrm{OCref}}}\right)^2 + \left(\frac{\mathbf{N}_\mathbf{I}(i) - \mathbf{O}_\mathbf{I}(i)}{I_{\mathrm{SCref}}}\right)^2}, \quad i = 1, \ldots, N, \tag{1}$$

where V_{OCref} and I_{SCref} denote the open circuit voltage and the short circuit current of the reference curve.

The maximum value of the error vector $E = \max(\mathbf{E}(i))$ is chosen as a qualitative comparison factor to obtain information on the maximum error between the two curves with i typically appearing close to the maximum power point (also seen in Figure 1).

2.2. The Solar Cell Model. The concept of scan time determination is based on a two-diode solar cell model extended by two parallel capacitances modelling the dynamic processes in

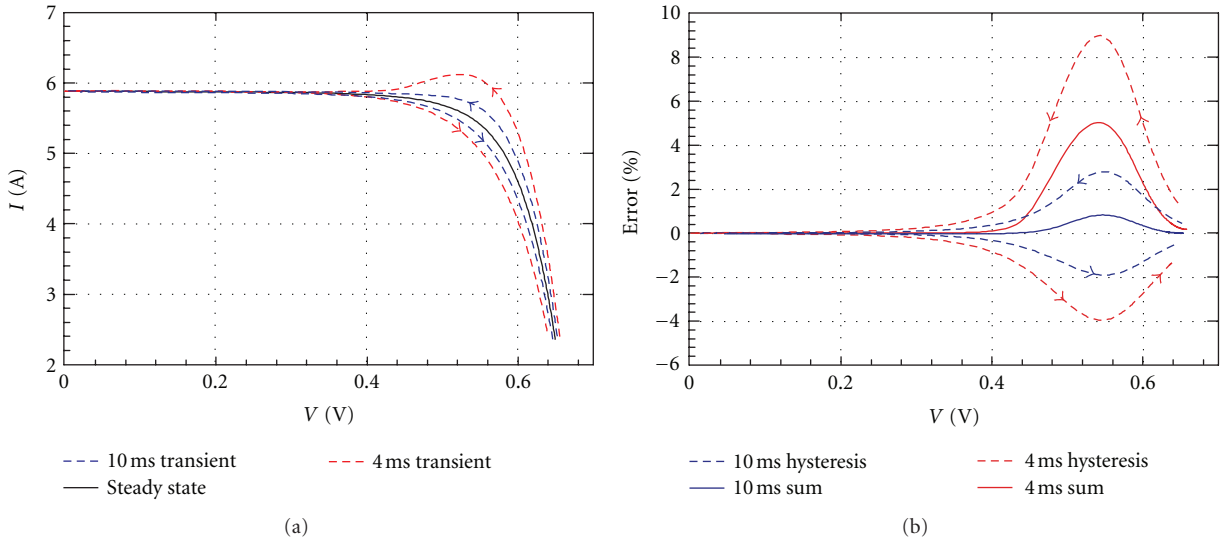

FIGURE 1: The I-V curve hystereses due to the forward and reverse sweep (a) and the corresponding errors caused by the internal capacitance (b) of a back-contacted monocrystalline silicon solar cell (arrows indicate the direction of the sweeps).

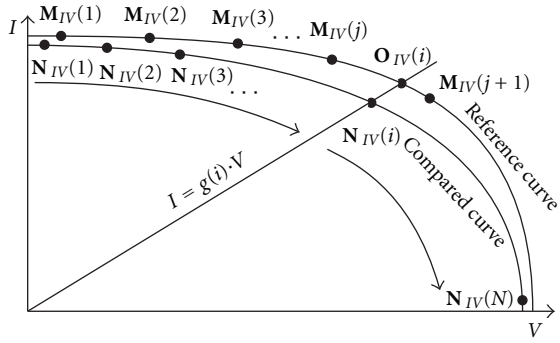

FIGURE 2: Error calculation geometry for a forward sweep.

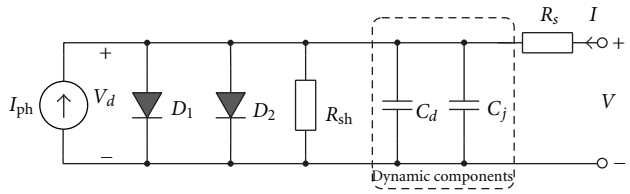

FIGURE 3: Two-diode solar cell model extended by two capacitances.

a solar cell (Figure 3). The two-diode model instead of a more common one-diode model is required for better accuracy of dynamic parameter extraction [9].

The model in Figure 3 consists of diodes D_1 and D_2 representing the Shockley diffusion direct current and the space charge recombination current, respectively, lumped shunt resistance R_{sh}, lumped series resistance R_s, junction capacitance C_j, diffusion capacitance C_d, and the photogenerated current under illumination I_{ph}. The diodes D_1/D_2 are modelled with the saturation currents I_{s1}/I_{s2} and the diode ideality factors n_1/n_2.

The capacitances C_d and C_j determine the dynamic properties of the SC under investigation. Assuming an abrupt p^+-n or n^+-p junction, an analytical approximation of the C_j is derived from the $C_j(V_d) = -dQ/dV_d$ equation [10]:

$$C_j(V_d) = \frac{C_{j0}}{\sqrt{1 - V_d/V_{bi}}}; \quad V_d < V_{bi}, \tag{2}$$

where C_{j0} is the junction capacitance at zero applied voltage, V_d is the internal solar cell voltage, and V_{bi} is the built-in potential. Such voltage-dependent capacitance, although limited as V approaches V_{bi}, is implemented into the SPICE diode model.

The C_d, as the key component of the SC's forward-biased dynamic character, is an outcome of minority charge carrier storage in the neutral region and its diffusion ability. C_d is proportional to the base minority carrier lifetime τ_d. For $V_d \gg kT/q$ (forward-biased solar cell), the C_d can be written as a function of temperature, applied voltage, and carrier lifetime using the following simplified equation [10]:

$$C_d(V_d) = \frac{q}{2n_1kT} I(V_d)\tau_d = \frac{q}{2n_1kT} I_S e^{qV_d/n_1kT}\tau_d, \tag{3}$$

where q is the electron charge, τ_d is the effective diode base minority carrier lifetime, and $I_S e^{(qV_d/n_1kT)}$ is the diode forward DC current. In the voltage range where $C_d \geq C_j$, the forward current of the diode D_1 is a few orders of magnitude higher than that of D_2; thus, only the current of the diode D_1 can be used in (3).

Measurement of C_d using direct C-V measurement is aggravated due to high solar cell currents in forward bias. More often, C_d is calculated from (3), while the lifetime τ_d is measured using one of the following methods: reverse recovery [11], short circuit current decay [12], or open circuit voltage decay (OCVD) [8]. During the OCVD measurement, the charge stored in the SC structure diminishes through

different loss mechanisms. The OCVD measurement starts with application of a predefined external current or voltage (forward bias) to the device under test (DUT). At $t = 0$, the forward bias is abruptly switched off. The voltage decay on the DUT's terminals is measured as the charge stored within the DUT diminishes with time. Voltage should be monitored as close to the DUT as possible to avoid the error caused by the series resistance of the measurement setup.

Three characteristic regions can be defined when analysing the OCVD signal of crystalline silicon SCs (see Figure 5 for OCVD shapes of different technologies) [13]:

(i) the voltage drop due to the lumped series resistance,

(ii) the quasilinear region due to the charge storage in neutral region (diffusion component),

(iii) the exponential decay that starts with the diffusion capacitance dropping below the junction capacitance. The charge stored in the space charge region is released through the recombination process and the lumped shunt resistance R_{sh}.

With both capacitances implemented and the static two-diode model parameters determined, we will present a method to extract both the τ_d and the C_{j0} parameters from the OCVD signal.

2.3. Extended Model Parameter Extraction. Two basic measurements—the *I-V* characteristic and the OCVD signal—are required for determination of the parameters of the extended model shown in Figure 3. As the OCVD signal is measured without the illumination, the method gives best results with the dark quasi static *I-V* measurement. Only the extraction of the photo-generated current I_{ph} is required under illumination.

Our measurement setup consists of an *I-V* curve tracer and an OCVD measurement setup. The curve tracer is constructed from parallel connection of three independent channels of two Keithley SMU 2602A units. One channel is configured as a voltage source determining the measurement voltage, whereas the other two channels are configured as current sources connected in parallel, extending the current range of the setup. All channels are interconnected with TSP link to provide single script output control. We programmed a measurement script that enabled automated measurements up to 1 V and 9 A with the worst-case voltage measurement accuracy of ±0.035% and the worst-case current measurement accuracy of ±0.18% [14]. The OCVD measurement setup is based on a 16-bit PCI6014 DAQ card controlling the switch and measuring the voltage decay. Sampling frequency is set to 200 kHz with the worst-case voltage measurement accuracy of ±0.031% [15].

Measurements under illumination were carried out on a temperature-controlled platform under a Newport class A continuous solar simulator. The STC conditions were met; the cell temperature regulation was maintained at 25°C by a temperature-stabilized measuring table [16], and the solar irradiance of 1000 W/m^2 was set using a calibrated reference solar cell with ±2% accuracy [17]. Following the acquisition of the required measurements, the algorithm starts with extraction of the two-diode static model parameters (I_{s1}, n_1, I_{s2}, n_2, R_s, and R_{sh}) from the measured *I-V* curve. Extraction of R_s is based on a method given in [18], where further improvements are implemented to optimize the accuracy of the dynamic model. A fully automated algorithm in MATLAB is developed that comprehends the following steps.

I. The influential range for the series resistance R_s, diode D_1, and diode D_2 on the input I-V curve is determined.

II. The series resistance R_s and the diode ideality factor n_1 are extracted using a bijective transformation and linear regression [18]. The inner solar cell potential $V_d = V - R_s I$ is calculated for further parameter extraction.

III. The D_1 diode's saturation current I_{s1} is calculated from the upper exponential region of the I-V curve. A derivative-free unconstrained simplex multivariable minimum search method is used to obtain the best fit [19] in the selected voltage range determined by the curve alignment function

$$\theta_{\text{RMS}} = \sqrt{\frac{\sum_{i=1}^{n} 2\log|I_{\text{meas}}(U_i)/I_{\text{model}}(U_i)|}{n}}. \tag{4}$$

The modelled curve is calculated at voltage points U_i of the measured curve. Index i runs through n measured points of the selected voltage range.

IV. The current of D_1 is subtracted from the total current. Both diode D_2 parameters are calculated from the lower exponential region of the remaining current using the same derivative-free unconstrained simplex multivariable minimum search method.

V. The shunt resistance R_{sh} is calculated as the derivative of the I-V curve at $V = 0$ and subtracted by the derivative of D_1 and D_2 characteristics [18].

VI. D_2 parameters are recalculated with a new target current. Both the D_1 and R_{sh} currents are subtracted from the total current.

VII. An additional step is added to fine-tune the diode D_1 parameters. I_{s1} and n_1 are recalculated to minimize the error in the range where the currents of both diodes are of comparable magnitudes.

Once the static parameters are known, we proceed with the extraction of the dynamic parameters (τ_d for C_d, C_{j0} for C_j). The effective lifetime τ_d can be extracted from the OCVD signal using the equation [20]

$$\tau_d = \frac{nkT/q}{dV/dt}, \tag{5}$$

where dV/dt is the slope of the linear part (region ii) of the OCVD signal. In the case of solar cells, where diffusion lengths approach the length of the base, the voltage decay is influenced by the base-emitter coupling effect causing the region ii to deviate from a straight line [20]. Extraction of τ_d from (5) is unreliable in such case. Our method uses (5) only for initial approximation of the simplex algorithm.

The initial approximation of the C_{j0} parameter can be calculated form (2) considering typical semiconductor parameters of the solar cell under investigation. Higher precision of C_{j0} is obtained from the low-bias region of the OCVD signal (region iii), where the exponential decay is driven only by C_j.

An unconstrained simplex multivariable minimum search optimization algorithm is used to minimize the error between the OCVD simulation and measurement. Best fit is obtained for both the τ_d and the C_{j0} parameters at the same time. The algorithm is implemented in MATLAB, where SPICE netlist is generated, and transient analysis is executed for each optimization step. Error between the measurement and simulation is calculated and passed back to the optimization algorithm. The extraction algorithm applied to the three test cells with the basic parameters shown in Table 1 yields the extended two-diode model parameters shown in Table 2 together with the static *I-V* RMS curve alignment factor.

2.4. Evaluation of the Extraction Method and the Extended Model. An accurate static model is required for accurate dynamic parameter extraction. However, there is no direct relation between the model and the parameter accuracies. The accuracy of the presented parameters in Table 2 is not relevant as the dynamic parameters are not calculated straightforward from the static parameters. It is the static *I-V* curve matching that is essential for good OCVD simulation agreement. We can show good static *I-V* curve alignment between model simulations and measurements, thus proving that such model is suitable for use over wide operating range of solar cells as seen in Figure 4. Accompanying curve alignment RMS errors defined by (4) are listed in Table 2 and range in the three cases from 0.0279 to 0.0491.

The quality of the dynamic model parameters can first be estimated by observing the degree of alignment between the simulated OCVD signal and the measured one. In the case of inaccurate dynamic (or static) model parameters, the simulated OCVD signal does not match the measured OCVD signal. Figure 5 shows a good alignment with slight deviations in the higher voltage range of mc-Si and BC mc-Si cells. Analysis showed that the deviations are a result of the base-emitter coupling effect that is not included in the dynamic model.

The minority carrier lifetimes are injection level dependent, especially when high injection levels are reached. However, in the range from 0.2 to 1, sun irradiance silicon-based solar cells are found in the low injection regime, where the lifetime does not vary significantly [21]. To verify the assumption, OCVDs of all test cells were measured at initial currents of 6 A, 4 A, and 2 A and compared to simulations using parameters extracted at short-circuit currents under STC (Table 2). The simulations were performed under equal conditions as the measurements, and the alignment is comparable to the alignment seen in Figure 5. From that, we can assume that a constant minority carrier lifetime can be used to analyse the effect of irradiance in the range from 1100 W/m^2 down to 200 W/m^2.

For the purpose of further evaluation, errors between several *I-V* scans with varied scan speeds versus a slower transient reference scan have been compared between measurement and simulation. A simple approach to vary the scan time of the *I-V* curve sweep from I_{SC} to V_{OC} is to vary the capacitance of a capacitive load. At $t = 0$, a power MOSFET connects the load capacitor to the DUT. The load capacitor starts charging with the initial current limited by the series resistance of the measurement circuitry including the series resistance of the load capacitor. To compensate the resistance and attain the short circuit current, a small negative initial charge is applied to the load capacitor prior to the measurement. During the *I-V* curve sweep, the current and voltage of the DUT are measured using two channels of the DAQ interface.

A series of measurements and simulations were performed on the three cells. Figure 6 presents some of them for the mc-Si cell (measurement B is omitted for better readability of the chart). The load capacitor values, the scan times, and the errors of both simulations and measurements are shown in Table 3.

The agreement between measurement and simulation is within the acceptable tolerance of ±0.1% with an exception of measurements C and D of the BC mc-Si cell. Solar cells with diffusion lengths approaching the physical length of the base encounter the base-emitter coupling effect that decreases the accuracy of the C_d model. The selected C_d model causes the error of such solar cells to be overestimated. The misalignment arises at higher error values and shorter scan times, whereas at measurement B, at error value of 1.4%, the mismatch error between measurement and simulation is still within ±0.1%.

In capacitive *I-V* curve measurement, as well as in semiconductor/resistive measurement, the scan speed has almost no effect on I_{SC}. Solar cell's dynamic error manifests in somewhat lower voltage reading on the DUT terminals. The voltage mismatch in the area near I_{SC} is detectable only in low-quality cells, where the shunt resistance creates a significant current slope. In regular quality cells, even though the voltage mismatch does exist, it is undetectable due to the almost constant *I-V* curve slope near I_{SC}. The V_{OC} on the other hand is strongly affected in semiconductor/resistive curve tracer systems but is not affected in capacitive-based tracer systems. As the capacitor is reaching its top charge, the current rate decreases, and the transient error fades away. Therefore, we can only observe the effect of scan speed on P_{MPP} shown in Table 3. As expected, the P_{MPP} is hardly affected in the pc-Si cell with mild dynamic character, whereas in the BC mc-Si cell due to the expressed diffusion capacitance, the measured maximal power at the fastest scan speed is significantly reduced.

2.5. The Generalized PV Module Model. PV modules are typically constructed from single cells connected in series. An equivalent generalized model can be introduced to model the PV module *I-V* characteristics using a small amount of circuit parameters [22]. In general, the characteristics of solar cells within a module should be as similar as possible

Table 1: Basic parameters of solar cells under investigation under STC.

Name	A, cm^2	I_{SC}, A	V_{OC}, V	FF, %	P_{mpp}, W	η, %
pc-Si	240	7.46	0.586	75.3	3.29	12.9
mc-Si	240	8.59	0.631	79.5	4.31	17.9
BC mc-Si	153	5.88	0.660	76.8	2.98	19.5

Table 2: Extracted model parameters of solar cells under investigation under STC.

Name	R_s, mΩ	R_{sh}, kΩ	I_{s1}, μA	n_1	I_{s2}, μA	n_2	τ_d, μs	C_{j0}, μF	θ_{RMS}
pc-Si	3.41*	2.85	0.104	1.293	1.68	4.240	5.0	12.5	0.0279
mc-Si	0.371	10.4	0.0288	1.260	0.150	3.588	35.0	5.0	0.0287
BC mc-Si	2.01*	0.115	0.204	1.543	0.420	4.550	240	1.0	0.0491

*Measured with soldered ribbons.

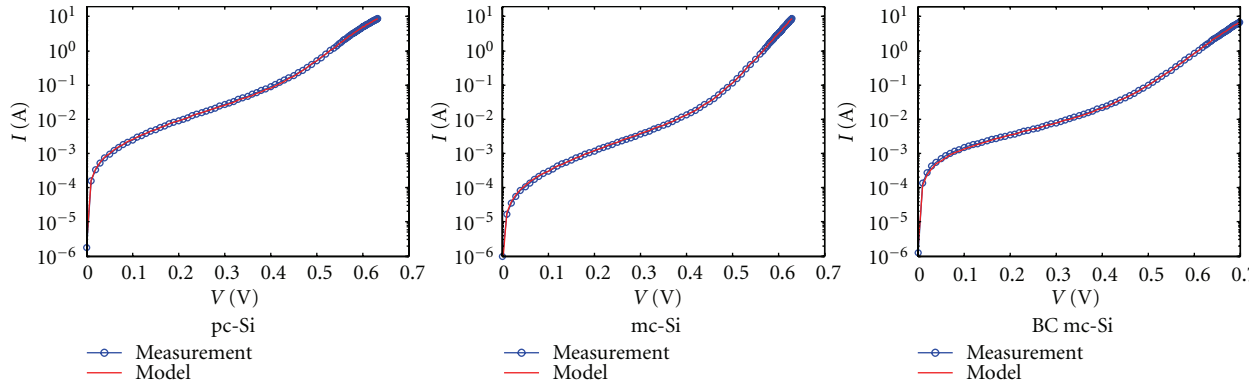

Figure 4: Alignment between modelled and measured I-V curves of selected solar cells shown in semilogarithmic scale.

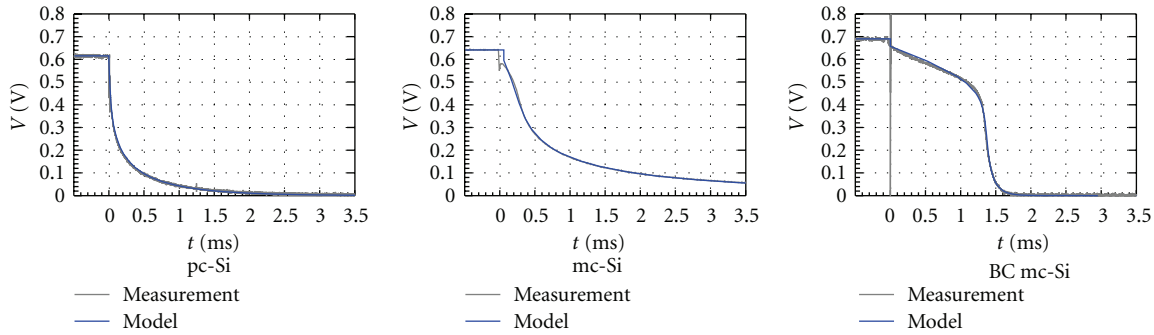

Figure 5: Alignment between modelled and measured OCVD signals of selected solar cells.

Table 3: Capacitive curve tracer I-V results: measurement versus simulation.

		Scan time/maximum power/measurement error/simulation error t, ms/P_{mpp}, W/E_{meas}, %/E_{sim}, %											
C_m [mF]	Meas.	pc-Si				mc-Si				BC mc-Si			
39.1 ± 2%	Ref.	22.0	3.30	—	—	20.5	4.29	—	—	27.1	2.90	—	—
28.5 ± 2%	A	17.1	3.29	0.2*	0.01	14.8	4.28	0.14	0.17	19.0	2.87	0.76	0.8
17.7 ± 2%	B	10.4	3.29	0.2*	0.05	9.1	4.26	0.21	0.26	10.8	2.82	1.34	1.41
11.6 ± 2%	C	7.2	3.28	0.2*	0.9	6.1	4.23	0.61	0.57	7.4	2.77	2.1	2.4
5.0 ± 2%	D	3.1	3.26	0.38	0.31	2.8	4.16	1.2	1.17	3.2	2.62	4.15	4.91

* s/n ratio too low for accurate error determination.

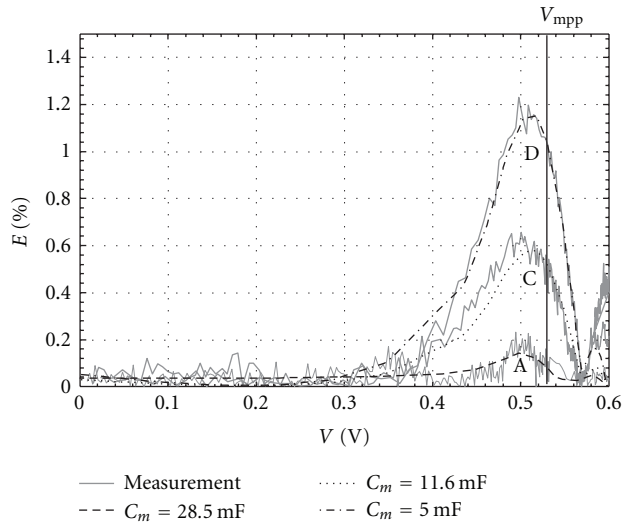

Figure 6: Voltage distribution of transient error for mc-Si cell.

to obtain the best module efficiency; thus, the theory of the generalized model assumes a PV module is constructed of N_s equal cells connected in series. The generalized one-diode static model characteristics are written as follows [22]:

$$I_M = I_{\text{ph}M} - I_S\left(e^{((qV_M - I_M R_{sM})/N_s nkT)} - 1\right) - \frac{1}{N_s} R_{\text{sh}M} I_M, \quad (6)$$

where indices M denote quantities referred to the module. The generalized model equals the diode model up to the factor of N_s. The same applies if a two-diode model is used instead.

In theory, the total module capacitance is $C_{dM}(V_M) + C_{jM}(V_M) = \left(\sum_{i=1}^{N_s}(C_{di}(V) + C_{ji}(V))^{-1}\right)^{-1}$. The junction capacitance at zero voltage equals $C_{j0M} = C_{j0}/N_S$ in the case of identical cells. In the case of nonidentical cells' C_{j0}, the total C_{j0M} equals parallel connection of individual C_{j0} values.

From (3) and (6), presuming equal τ_d of all cells, the C_d can be expressed as

$$C_{dM}(V_M) = \frac{q}{2N_S nkT} I_S \, e^{((qV_M - I_M R_{sM})/N_S nkT)} \tau_d, \quad (7)$$

in the case of a PV module. As expected, the value of the minority carrier lifetime withholds the value of a single cell, whereas the total capacitance reduces by the factor N_S.

A test module with access to all interconnections between the individual cells (built of 4 monocrystalline silicon SCs shown in Figure 7) was laminated in our laboratory. Validation of the method for the dynamic parameter extraction of a PV module is carried out through the distribution of the dynamic components along the module. Figure 8 displays the OCVD measurement of the individual cells, the sum of the individual measurements, and the OCVD measurement of the entire module.

Very good agreement between the sum and the module OCVD response with deviation only at times $t < 0$ s can be observed. This deviation arises from the series resistance of bus bars used to contact the cell interconnections. The

Figure 7: An experimental 4-cell mc-Si module (dashed circles mark access to external and individual cell contacts).

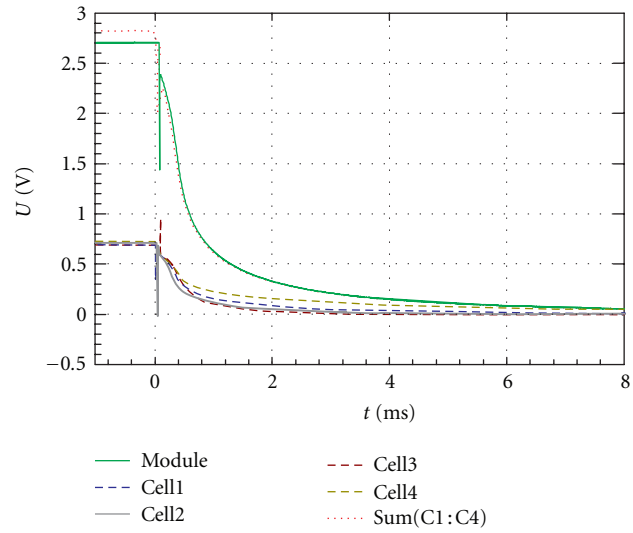

Figure 8: OCVD signal of the 4-cell mc-Si module and its individual cells.

actual series resistance of the module is determined from the I-V measurement and is properly considered in the dynamic parameter extraction method. The OCVD signal of the module equals the sum of the individual responses of SCs involved; therefore, in the OCVD signal of the PV module each solar cell contributes its share of charge proportional to its total internal capacitance. The OCVD signal of the PV module can thus be used to extract C_{j0M} and τ_{dM} parameters, where C_{j0M} should equal the parallel connection of the individual C_{j0} values, and τ_{dM} should equal the average value of the individual τ_d values. The individual values of C_{j0M} and τ_{dM}, however, should not diverge considerably from each other.

Table 4 displays results of the parameter extraction method applied to the individual cells and to the module. Most results calculated from individual cells are in good agreement with the theory. The discrepancy in the R_s can be explained through the resistance of additional bus bar length required to contact individual cells. The second discrepancy, found in I_{S2}, is caused by cell 4 with parameter I_{S2} unfortunately significantly smaller compared to the other

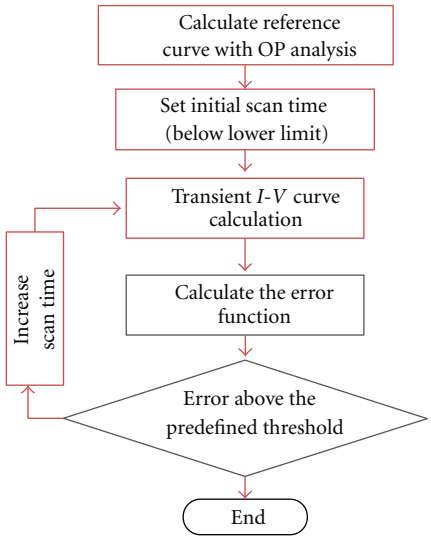

Figure 9: Scan time extraction algorithm.

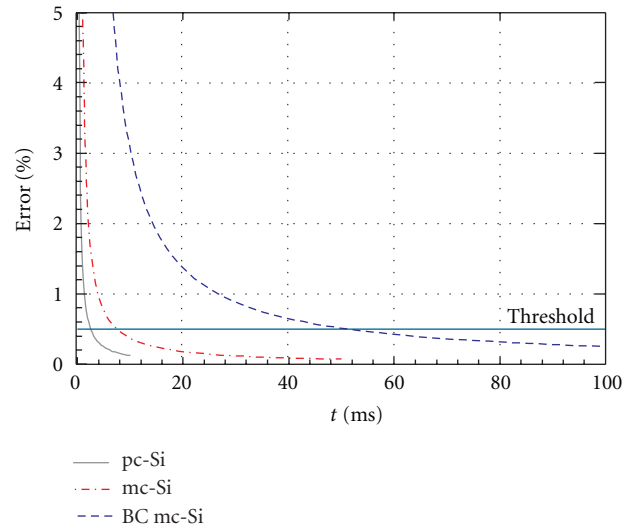

Figure 10: Error versus scan time for the three cells under investigation.

cells. In such case, the effective I_S is not determined by the smallest I_S value.

However, the extracted dynamic parameters are determined within the expected range of tolerance, and extraction process can be used to determine the generalized two-diode model for PV modules when cells with similar properties are involved, which is the case in all high-efficiency PV modules.

3. Scan Time Determination

The minimum scan time of a single cell or a PV module at a predefined error threshold can be determined by an iterative algorithm from a series of transient I-V curve simulations. The dynamic model of the DUT is used for both the reference and the compared curve simulations. The reference curve is simulated by sweeping the operating point (OP) analysis to eliminate the capacitance effects, whereas the compared curves are simulated using transient analysis. The numerical computation and netlist generations are handled in MATLAB, whereas SPICE is executed within MATLAB for circuit simulations (Figure 9).

In the process of determination of the maximal tolerable predefined error threshold, other sources of I-V curve errors as well as the ratio of the required scan time to the I-V curve error should be considered. It is reported that specialized laboratories are able to achieve I-V curve measurement uncertainties from 1.6% to 3% [3]. Also in Figure 10, we can observe a quasiexponential decrease of error versus scan time leading to very long scan times at low error thresholds. Determination of the predefined error depends strongly on the purpose of the measurement. To stay at least a factor of 3 below other uncertainties and to avoid too long scan times (Figure 10), the predefined error threshold was set at 0.5%. Rendered optimum scan times are 2.2 ms, 7.3 ms, and 43.8 ms for the pc-Si, mc-Si, and BC mc-Si solar cells, respectively.

4. Effect of Irradiance Level

4.1. Experiment Background and Expectations. In the study of the influence of irradiance (G) on the scan time, the RC time constant τ_C, causing the delay when sweeping the I-V curve from point to point, should be calculated. In forward bias, the C_d dominates the total cell capacitance, and the current through the D_2 is negligible. When sweeping the I-V curve using a voltage source, the time constant is defined as

$$\tau_C = RC = \frac{C_d}{g_s + g_{\text{sh}} + g_d}, \tag{8}$$

where $gs = 1/R_s$, $g_{\text{sh}} = 1/R_{\text{sh}}$, and g_d is differential conductance of the diode D_1 between the neighbouring points. The following equation can be derived using simplified equations for C_d and g_d [10] and assuming that $g_{\text{sh}} \ll g_s$:

$$\tau_c = \frac{\tau_d}{2} \frac{I_{d1}}{(I_{d1} + g_s V_T)}. \tag{9}$$

I_{d1} is the current flowing through the diode D_1 (Figure 3), and V_T is the thermal voltage. Equation (9) implies that the time constant is slightly increasing with diode current. The current I_{d1} is the difference between the photogenerated current and the current flow out of the device terminals ($I_{d1} = I_{\text{ph}} - I$). At V_{OC}, where $I = 0$ A, the decrease in irradiance yields lower time constants and thus smaller transient errors.

The trend of τ_C can be observed in a step response of the measured device. A simulation in V_{OC}, where the time constant is maximal, with a step amplitude of 0.01 V, has been performed at different currents I_{d1}. A sweep of I_{d1} is used to model the change in irradiance. The stationary V_{OC} conditions have been established by a large capacitor in series with a step voltage source.

Simulation in Figure 11 confirms the (9). A decrease in irradiance yields shorter step responses and shorter time

Table 4: Extracted parameters of individual cells and module (monocrystalline silicon solar cells).

Cell	R_s, mΩ	R_p, kΩ	I_{s1}, μA	n_1	I_{s2}, μA	n_2	τ_d, μs	C_{j0}, μF
Cell 1	6.251	5.0	5.65	1.15879	141.0	3.64096	35.0	4.50
Cell 2	9.693	1.2	5.77	1.16285	446.0	4.38751	35.0	5.70
Cell 3	7.086	5.0	3.80	1.13891	696.0	5.10632	45.0	5.30
Cell 4	10.216	6.3	5.15	1.15259	33.9	2.98760	45.0	4.70
Module calculated	33.246	17.5	3.80	4.61314	33.9	16.12239	42.5	1.25
Module measured	23.039	17.0	3.49	4.53281	183.0	14.32319	41.3	1.43

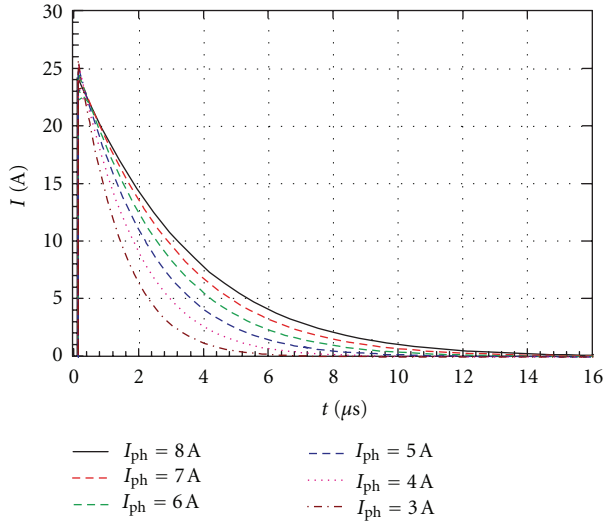

Figure 11: Simulated step response of mc-Si solar cell.

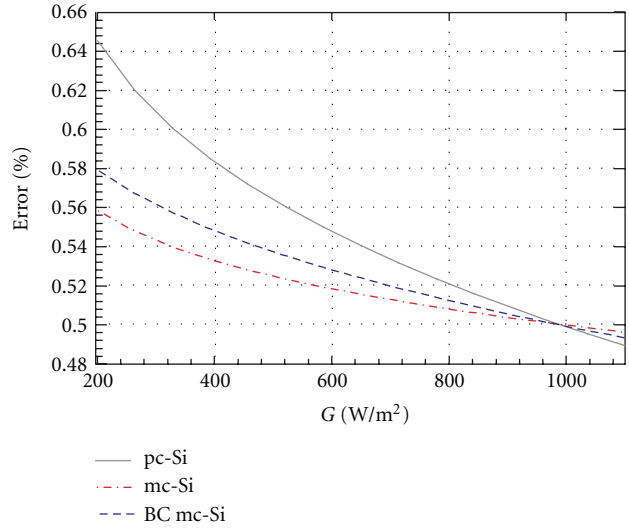

Figure 12: Effect of irradiance variation on transient error.

constants. At first sight, the decrease of the time constant should also decrease the *I-V* curve error. However, as follows, there is more to the transient error than just the time constant.

4.2. Effect of Irradiance on I-V Curve Error. The source of the transient error is the capacitance that introduces the time constant τ_C. As soon as the capacitance is present in the circuit, there are several factors aside the time constant affecting the magnitude of the error.

(i) The duration of *I-V* scan severely impacts the error: each time the load changes, the capacitor charge needs to be equalized. The transient error directly depends on dV/dt between consequent scan points. When the same sweep algorithm is involved, what matters is the total time to sweep from I_{SC} to V_{OC}, regardless of the number of points.

(ii) The *I-V* curve sweep algorithm: achieving a homogenous density of *I-V* curve points is a common issue. Constant current (or voltage) step yields approximately equidistant point distribution from the maximum power point to V_{OC} (or to I_{SC}) and only a few points in the other direction. Different approaches are used to acquire equidistant point distribution along the curve such as logarithmic voltage step, combined voltage and current stepping, adaptable on the fly step calculation. Whichever method is used, they all vary dV/dt throughout the *I-V* curve.

(iii) Lastly, the method of error determination also affects the *I-V* curve error: strictly considering the time constant, both points being compared should be selected at the same time of the measurement. However, the *I-V* curve does not contain the time information and has to be compared according to the equal power availability. Furthermore the direct comparison of two curves at different irradiance is impossible due the modified I_{SC}, the V_{OC}, and the entire curve path.

The error is thus determined using the method from Section 2 between a transient simulation and a quasi static operating point analysis (the ideal reference *I-V* curve). The scan time for each DUT is determined from the predefined error threshold of 0.5% at STC. The variation of irradiance in simulations is modelled through variation of the photogenerated current I_{ph}.

The *I-V* curve error versus irradiance for all three cells under test (Figure 12) surprisingly yields a result of reversed error/irradiance dependency. The sweep is performed at a high-density constant voltage step rate to exclude the

error arising from this source. Although the time constant decreases with decreasing irradiance, the error and consequently the optimal scan time moderately increase. The reverse trend arises from calculation of the relative error value. The effects of V and I can be evaluated separately. First, we focus on the relative current error calculation. At decreasing irradiance, the absolute error of current (δI) slightly decreases due to the fall of τ_C (9). For calculation of the relative error, the δI is divided by the short circuit current I_{SC}, which also decreases with the irradiance. Assuming, $I_{ph} \approx I_{SC}$, the reduction of I_{SC} is more rapid than the reduction of δI, which is proportional to the τ_C. Consequently, the overall error increases although the time constant decreases with irradiance. The actual error defined in (1) is an aggregate of the relative current error and the relative voltage error. The open circuit voltage varies only minor in observed irradiance range; thus, the trend of error versus irradiance mostly reflects the trend of relative current versus irradiance.

As the desired output of an error function is certainly a relative value of the I-V curve error, a moderate increase of error at lower irradiance levels should be considered at scan time determination procedure, in particular at outdoor monitoring sites. In scope of the three tested cells of different silicon technologies, the maximum relative deviation of error was 32% for the polycrystalline silicon solar cell at irradiance level of 200 W/m^2 compared to 1100 W/m^2.

5. Conclusions

A method of optimal I-V curve scan time determination of solar cells and modules based on the extended two-diode model was presented. An algorithm acquiring the parameters of the presented model from two simple measurements, an I-V scan and an OCVD signal, has been introduced. A newly introduced error determination function is used to estimate the mismatch between two I-V curves. Different aspects on determination of the tolerable predefined I-V curve error threshold caused by the PV generator's dynamic character were analysed. The predefined error threshold served as a base for the optimal scan time determination. The proposed extraction method has been applied but is not limited to different wafer-based solar cells and modules. Validation was achieved using capacitor-based I-V curve measurement, where different scan times were accomplished by variation of the load capacitance. The extraction method gives good results, whereas there is still some space for dynamic model improvement (PV generators with high minority carrier lifetimes). I-V curve error versus scan time dependency has been analysed where at error threshold of 0.5% scan times diverge from 2.2 ms up to 43.8 ms for DUTs of different silicon solar cell technologies. Therefore, the capacitive character of a DUT should certainly be considered prior to I-V curve measurement.

Even though the capacitance and the time constant of PV generators decrease with decreased irradiance, an increase of the error was ascertained. Mostly due to the relative current error, a moderate relative increase of 32% above the predefined 0.5% error threshold for the poly-crystalline solar cell under test was determined. When very high-precision measurements are required, such increase of error can affect the final measurement. The scan time should either be determined at the lowest expected irradiance level or a sufficient threshold error tolerance should be considered at the highest level of irradiance.

Acknowledgment

The authors would like to thank for the financial assistance given by the Slovenian Research Agency (P20197). M. Herman would personally like to acknowledge the Slovenian Research Agency for providing him with Ph.D. funding.

References

[1] C. Monokroussos, R. Gottschalg, A. N. Tiwari, G. Friesen, D. Chianese, and S. Mau, "The effects of solar cell capacitance on calibration accuracy when using a flash simulator," in *Proceedings of the IEEE 4th World Conference on Photovoltaic Energy Conversion*, pp. 2231–2234, May 2006.

[2] M. Prorok, W. Kołodenny, T. Zdanowicz, R. Gottschalg, and D. Stellbogen, "Reducing uncertainty of PV module temperature determination based on analysis using data gained during outdoor monitoring," in *Proceedings of the 23rd European Photovoltaic Solar Energy Conference*, D. Lincot, H. Ossenbrink, and P. Helm, Eds., 2008.

[3] N. Taylor, *Guidelines for PV Power Measurement in Industry*, Publications Office of the EU, 2010.

[4] International standard: IEC 60904-1 Ed.2: Photovoltaic devices—part 1: measurement of photovoltaic current-voltage characteristics. 2006.

[5] International standard: IEC 60904-10 Ed. 1.0 b:1998, Photovoltaic devices—part 10: methods of linearity measurement. Multiple. Distributed through American National Standards Institute (ANSI), 2007.

[6] G. Friesen and H. A. Ossenbrink, "Capacitance effects in high-efficiency cells," *Solar Energy Materials and Solar Cells*, vol. 48, no. 1–4, pp. 77–83, 1997.

[7] F. Recart and A. Cuevas, "Application of junction capacitance measurements to the characterization of solar cells," *IEEE Transactions on Electron Devices*, vol. 53, no. 3, pp. 442–448, 2006.

[8] R. Salach-Bielecki, T. Pisarkiewicz, T. Stapiński, and P. Wójcik, "Influence of junction parameters on the open circuit voltage decay in solar cells," *Opto-Electronics Review*, vol. 12, no. 1, pp. 79–83, 2004.

[9] M. Herman, M. Jankovec, and M. Topič, "A method for determination of I-V curve scan time of solar cells," in *Proceedings of the 47th International Conference on Microelectronics, Devices and Materials and the Workshop on Organic Semiconductors, Technologies and Devices*, pp. 207–211, 2011.

[10] S. Sze, *Physics of Semiconductor Devices*, Wiley-Interscience, Hoboken NJ, USA, 3rd edition, 2007.

[11] S. R. Dhariwal, "Measurement of lifetime of photoinjected carriers in solar cells by reverse voltage pulse response," *Solid-State and Electron Devices, IEE Proceedings I*, vol. 127, no. 1, pp. 20–24, 1980.

[12] K. Burgard, W. Schmidt, and W. Warta, "Applicability of electrical short circuit current decay for solar cell characterization: limits and comparison to other methods," *Solar Energy Materials and Solar Cells*, vol. 36, no. 3, pp. 241–259, 1995.

[13] M. P. Deshmukh and J. Nagaraju, "Measurement of silicon and GaAs/Ge solar cells ac parameters," *Solar Energy*, vol. 78, no. 1, pp. 1–4, 2005.
[14] "Keithley Model 2601A/2602A SourceMeter Specifications," 2012, http://www.keithley.com/data?asset=52059.
[15] "NI PCI-6013, PCI-6014 Multifunction DAQ specifications," 2012, http://digital.ni.com/worldwide/china.nsf/c362761bd12fc417862564bc006784d3/06897f85067a745686256c1b006cb50d/$FILE/PCI-6013-6014.pdf.
[16] F. Granek and T. Zdanowicz, "Advanced system for calibration and characterization of solar cells," *Opto-Electronics Review*, vol. 12, no. 1, pp. 57–67, 2004.
[17] WPVS Reference Cells—Fraunhofer ISE, 2012, http://www.ise.fraunhofer.de/en/service-units/callab-pv-cells-callab-pv-modules/wpvs-reference-cells.
[18] A. Kaminski, J. J. Marchand, A. Fave, and A. Laugier, "New method of parameters extraction from dark I-V curve," in *Proceedings of the IEEE 26th Photovoltaic Specialists Conference*, pp. 203–206, Calif, USA, October 1997.
[19] W. H. Press, S. A. Teukolsky, W. T. Vetterling, and B. P. Flannery, *Numerical Recipes: The Art of Scientific Computing*, Cambridge University Press, 3rd edition, 2007.
[20] P. W. Hawkes, *Advances in Electronics and Electron Physics*, Academic Press, 1986.
[21] J. O. Schumacher and W. Wettling, "Device physics of silicon solar cells," in *Clean Electricity from Photovoltaics*, Imperial College Press, 2001.
[22] L. Castañer and S. Silvestre, *Modelling Photovoltaic Systems Using PSpice*, J. Wiley, Hoboken, NJ, USA, 2002.